Nanoscale

PAPER

View Article Online
View Journal | View Issue

Cite this: *Nanoscale*, 2018, **10**, 17671

Steered molecular dynamics simulations reveal a self-protecting configuration of nanoparticles during membrane penetration†

Yousef Nademi, [a] Tian Tang *[b] and Hasan Uludağ *[a,c,d]

Received 27th May 2018,
Accepted 23rd August 2018

DOI: 10.1039/c8nr04287j

rsc.li/nanoscale

Cell entry of polynucleotide-based therapeutic agents can be facilitated by nanoparticle (NP) mediated delivery. In this work, using steered molecular dynamics simulations, we simulated the membrane penetration process of a NP formed by 2 short interfering RNA (siRNA) and 6 polyethylenimine (PEI) molecules. To the best of our knowledge, this is the first set of simulations that explore the direct penetration of an siRNA/PEI NP through a membrane at an all-atom scale. Three types of PEI molecules were used for NP formation: a native PEI, a PEI modified with caprylic acids and a PEI modified with linoleic acids. We found that hydrogen bond formation between the PEIs and the membrane did not lead to instability of the siRNA/PEI NPs during the internalization process. Instead, our results suggested adoption of a "self-protecting" configuration by the siRNA/PEI NP during membrane penetration, where the siRNA/PEI NP becomes more compact and siRNAs become aligned, leading to more stable configurations while detaching from the membrane. The siRNA/PEI NP modified with linoleic acid showed the smallest structural change due to its strong intra-particle lipid associations and the resulting rigidity, while NP modified with caprylic acid showed the largest structural changes. Our observations provide unique insight into the structural changes of siRNA/PEI NPs when crossing the cell membrane, which can be important for the design of new NP carriers for nucleic acid delivery.

1. Introduction

Gene therapy using polynucleotide-based therapeutic agents is a promising strategy that has attracted immense attention during the past decade.[1–3] For functional delivery, carriers are needed in order to facilitate translocation of polynucleotides through the plasma membrane as well as protection of polynucleotides from degradation.[4] Synthetic cationic polymers, due to their safety and versatility, are the commonly utilized carriers for gene delivery.[5] For therapeutic benefits, administered nucleotide/polymer nanoparticles (NPs) must be internalized by the targeted cells while retaining their integrity, and then polynucleotides need to disassemble from the polymeric carrier for transport to the appropriate sub-cellular compartment. Among synthetic carriers, polyethylenimines (PEI) have gained a central role in gene delivery with the advantage of being easily modified with functional groups, which makes it possible to tailor their properties for various applications.[6] A high molecular weight (HMW) PEI (~25 kDa) is often considered as a 'gold standard' in non-viral gene delivery; however, it manifests considerable toxicity by damaging the plasma membrane of the cells.[7] A low molecular weight (LMW) PEI (<2 kDa) displays an acceptable level of toxicity, but it has a low efficiency in gene delivery. Modification of LMW PEI with hydrophobic groups significantly increases cellular uptake and facilitates the entry to cells by promoting hydrophobic interactions with membrane lipids.[8,9] The beneficial effect of the hydrophobic modifications depends on the nature of the substituted lipids and the level of substitution.[9]

The first stage of NP delivery into the cells is cellular uptake, which usually occurs through two pathways: active endocytosis and direct penetration.[10] Direct penetration is a non-endocytic translocation pathway, where a NP crosses the cell membrane without the need to be confined by the endocytosis vesicles. Compared with endocytosis, direct penetration is a less frequent event, but it can occur through diffusion, permeation and pore formation. Small NPs (<1 nm) may cross cell membranes by passive diffusion through specialized transport protein channels existing on the cell membrane.[11]

[a]Department of Chemical and Materials Engineering, University of Alberta, Edmonton, Canada. E-mail: hasan.uludag@ualberta.ca
[b]Department of Mechanical Engineering, University of Alberta, Edmonton, Canada. E-mail: tian.tang@ualberta.ca
[c]Department of Biomedical Engineering, University of Alberta, Edmonton, Canada
[d]Faculty of Pharmacy and Pharmaceutical Sciences, University of Alberta, Edmonton, Canada

† Electronic supplementary information (ESI) available. See DOI: 10.1039/c8nr04287j

Intermediate sized NPs can permeate across cell membranes without inducing a distinct pore in the membrane structure. Such a mechanism was proposed for polymeric NPs with appropriate hydrophobicity[12,13] such that the NP experienced repulsion from both the solvent and the membrane tail. In this case, frequent exchange occurred between the polymer adsorption onto the membrane and desorption back into the solvent, which increased fluctuations in the lipid bilayer and eventually enhanced NP permeability.

Translocation by transiently induced pores is another direct penetration method, where pores are induced by various approaches including electroporation, mechanical stress, shock waves (sonoporation), surface-active molecules, small cationic peptides, and cationic polymers.[14] In electroporation, pores are induced by applying external electric fields. Tieleman *et al.*,[15] using molecular dynamics (MD) simulation, found that the external electric field interacted with water dipoles, increased the probability of forming water defects in the membrane interior, and stabilized the formed defects. Pore-mediated translocation can also be enabled by the application of shock waves such as high pressure waves that propagate at a supersonic speed and pass through the cell membranes within several picoseconds.[16] While the process of pore formation due to shock waves is still not fully understood, Koshiyama *et al.*[17] proposed that shock waves caused structural changes in the lipid bilayer such as bilayer thinning and disordering of lipid chains, which led to the penetration of a considerable amount of water molecules into the hydrophobic core of the bilayer and eventually the formation of a hydrophilic pore. Some surface-active molecules with covalently bonded hydrophilic and hydrophobic groups may also induce a pore in the membrane structure.[14] For example, MD simulations[18] revealed that dimethylsulfoxide (DMSO), containing a hydrophilic sulfoxide group and two hydrophobic methyl groups, could readily penetrate into a lipid/water interface, which led to bilayer expansion and loss of lateral interactions between the lipid head groups. Consequently, thermal fluctuations at the lipid/water interface caused structural defects and eventually a pore in the membrane. Small cationic peptides can also induce pores in membranes *via* different mechanisms. As an example, Leontiadou *et al.*[19] through their MD simulations proposed a cooperative pore formation mechanism for the cationic (+3) magainin MG-H2 peptide which is an antimicrobial peptide. Upon binding to the membrane surface, the peptide molecules aggregated and oriented themselves in a way such that their hydrophobic side chains interacted with the membrane lipid tails while their charged lysine residues remained bonded with the membrane head groups. As a result, the fluctuation in the lipid/water interface increased, triggering the contact between peptide lysine residues and water molecules on the other side of the lipid bilayer, and finally leading to the formation of a hydrophilic pore. Some cationic polymers such as polyamidoamine (PAMAM) dendrimers were also shown to induce pores in membrane structures.[20] It was observed[20] that after initial binding to the membrane surface, the charged moieties of the dendrimer penetrated into the lipid/water interface, and made contact with lipid head groups of the opposite leaflet, causing pore formation.

These simulations focused on pore formation by external fields or small polymeric molecules. Although direct penetration is most efficient for NPs of <50 nm diameter,[21] NPs as large as 100 nm have also been internalized using this method.[21] It is therefore of interest to investigate the membrane penetration of polynucleotide/polymer NPs employed in gene delivery. While previous MD simulations have provided critical insights into the nucleic acid complexation with the carriers,[6,22–24] simulations on NP penetration across membranes were performed almost exclusively at the coarse-grained (CG) level,[25–29] which are incapable of revealing atomistic details behind effective carriers. To the best of our knowledge, no studies at the all-atom level have simulated the membrane penetration of polynucleotide NPs. However, we found three all-atom studies that investigated the interaction of either PEI or deoxyribonucleic acid (DNA) alone with a lipidic bilayer.[30–32] Antipina *et al.*[31] utilized an umbrella sampling method to study the free energy profile of a bare 22 b.p. DNA across a palmitoyloleoylphosphatidylcholine (POPC) lipid bilayer. They observed that as the DNA approached and crossed the zwitterionic lipid bilayer, the free energy monotonically increased, which indicated the lack of attraction between the DNA and the zwitterionic lipid bilayer. This study confirmed that the anionic DNA requires a cationic vector to facilitate its interaction with the membrane. Kwolek *et al.*[30] simulated the interaction of a PEI with POPC and POPC/1,2-dioleoyl-*sn-glycero*-3-phosphoric acid (DOPA) lipid bilayers. It was observed that the PEI interacted with the lipid bilayers mainly by the hydrogen bond (HB) formation between the PEI amine groups and Os in the phosphate or ester groups of the lipids. Choudhury *et al.*[32] utilized MD simulation to assess how linear PEI (lPEI) in different protonation states (complete *vs.* partially protonated N atoms) interacts with dioleoylphosphatidylcholine (DOPC) lipid bilayers. Their simulation showed that at low pH, lPEI chains formed an elongated conformation due to the electrostatic repulsion between the protonated N atoms, and induced water/ion channels through the membrane. Unprotonated lPEI, on the other hand, was highly coiled and predominantly remained at the bilayer–water interface.

While these studies on the individual constituents of polynucleotide NPs may be beneficial, it is evident that further studies are required to provide atomistic insight into the membrane penetration of polynucleotide NPs. In this work, we applied steered molecular dynamics (SMD) simulation to examine the membrane penetration of a polynucleotide NP formed by small interfering ribonucleic acid (siRNA) and PEI molecules. A zwitterionic POPC lipid membrane was used as a model of cellular membranes. The siRNA/PEI NPs were steered by applying a moving constraint to cross the membrane structure. The SMD simulation serves not only to accelerate the penetration process, which is difficult to observe under standard MD simulation for such large and complex NPs, but also

to mimic the situation where the NPs are pulled by external or biophysical forces towards the interior of the cell membrane. Our focus in this study is not to reveal the specific forces that drive NP internalization, but rather to investigate the: (i) stability and structural changes of siRNA/PEI NPs, (ii) pore formation across a membrane and its stability, and (iii) effect of lipid groups on PEI during the penetration. A native and two additional PEIs modified with caprylic acid (CA) and linoleic acid (LA) were adopted here as the polynucleotide carriers.

2. Methods

2.1. Simulated systems and procedure

Three NPs are simulated each composed of 2 siRNA molecules and 6 branched PEIs (bPEIs). The simulated siRNA had the following sequence: sense: 5′-CAGAAAGCUUAGUACCAAATT-3′, antisense: 5′-UUUGGUACUAAGCUUUCUGTC-3′, which was used to silence *P*-glycoprotein.[9,33,34] It is composed of 42 nucleotides that carry a total charge of −40 in its fully deprotonated state. The simulated bPEI, in its native form, has a MW of 1874 Da (ref. 23) and consists of 43 amino groups, 20 of which are protonated corresponding to the protonation ratio of 47% at pH = 6 as reported by Utsuno and Uludağ.[35] This pH is selected due to the fact that siRNA based therapeutics are utilized to target cancer cells, and the extracellular pH of human tumors is known to be slightly on the acidic side.[36,37] The chemical structures and protonation sites of the simulated bPEI as well as structures of lipid substitutions (LA and CA) are shown in Fig. 1. The simulated NPs are referred to as LA-NP, where each PEI is modified with 3 LA substitutions; CA-NP, where each PEI is modified with 3 CA substitutions; and native NP, where the PEIs are not modified. These substitutions are in line with the practical range in which functional differences were seen from the native PEI in siRNA delivery.[9]

The initial structures of NPs were adopted from a previous study[22] after 200 ns production run. Each of the original systems included 4 siRNAs and 18 PEI molecules, from which we selected 2 siRNAs and 6 PEIs. Then, to equilibrate the structures, each NP was solvated with TIP3P[38] water molecules and ions (150 mM KCL) and subjected to 5 ns (restrained) + 45 ns (free) simulation with the MD package of NAMD.[39] The structure of each NP at the end of the simulation was adopted as the initial configuration of NPs for SMD simulations of membrane penetration.

The zwitterionic bilayers of 920 POPC molecules were constructed using a VMD[40] Membrane Builder plugin. The chemical structure of the POPC lipid bilayer is shown in Fig. 1. Upon

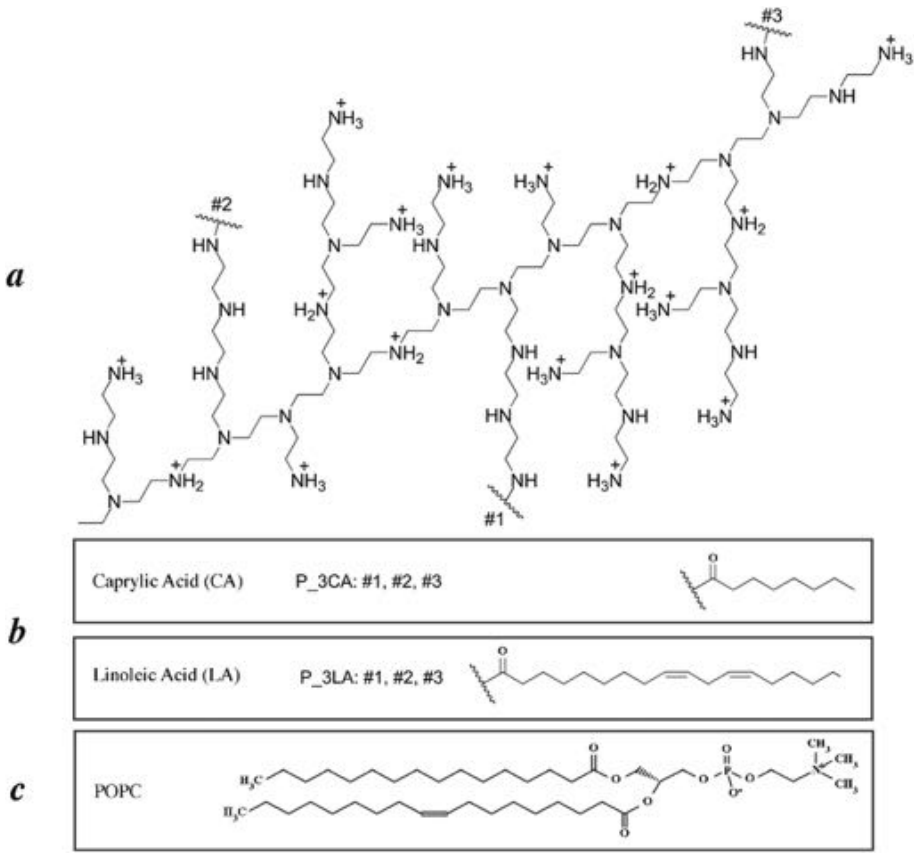

Fig. 1 (a) Molecular structure, protonation sites and lipid substitution sites of the simulated PEIs, (b) structures of the 2 substituted lipids, and (c) structure of the POPC molecule.

solvation with appropriate amounts of ions (150 mM KCl) and TIP3P[38] water molecules, the structure of the POPC lipid bilayer was equilibrated for 50 ns until the area per lipid of 63.06 ± 0.53 Å (data collected from last 20 ns) was obtained which is in agreement with the experimental values (63–68.3 Å per lipid).[41–43] The final configuration of the POPC lipid bilayer was then adopted as the input structure for SMD simulation with NPs. To facilitate the discussion, we will refer to the POPC lipid bilayer as the membrane. To prepare the membrane–NP systems for SMD simulation, each NP was placed above the membrane so that the center of mass (COM) distance between the membrane and the NP was 8 nm. Next, upon solvation with appropriate amounts of ions (150 mM KCl) and TIP3P[38] water molecules, the three membrane–NP systems were equilibrated for 10 ns with a harmonic restraint of 10 kcal mol^{-1} A^{-2} exerted on the non-H atoms of the NP. The equilibrated systems were then used for SMD simulations.

In a typical SMD simulation, the system is pulled along a certain direction by imposing a constant force or velocity on the simulated structure.[44] Here we used the constant velocity approach, where the COM of the NP was attached to a dummy atom *via* a virtual spring. The dummy atom was moved with a constant velocity in the z direction perpendicular to the membrane surface, and the force between the COM of the NP and the dummy atom is calculated using the following equations:

$$U = \frac{1}{2}k[vt - (\mathbf{r} - \mathbf{r}_0) \cdot \mathbf{n}]^2 \quad (1)$$

$$F = -\nabla U \quad (2)$$

where U is the potential energy, k is the spring force constant, v is the speed of pulling, t is the current time, $\mathbf{r}$ is the current position vector of the COM of the NP, $\mathbf{r}_0$ is the initial position vector of the COM of the NP, and $\mathbf{n}$ is the unit vector indicating the direction in which the dummy atom is pulled. Pulling speeds in the range of 0.1 to 100 Å ns^{-1} have been reported in the literature for constant velocity SMD simulation, while lower values of v have been used to estimate the potential of mean force (PMF) from SMD trajectories.[45–48] Results reported in this work are based on the value of v = 2.5 Å ns^{-1}, while the influence of the v value is briefly discussed later. The spring force constant k was set to be 5 kcal mol^{-1} Å^{-2} according to the "stiff-spring approximation".[47] Each SMD simulation took 64 ns to complete. Detailed information on the simulated systems in this study is given in Table 1.

2.2. Simulation details

The force field for the PEI molecules was adopted from a previous study[22] by our group which was generated based on the CHARMM General Force Field and validated with *ab initio* calculations. A CHARMM 36[49,50] Force Field was used for all other molecules. The TIP3P[38] model was used for water molecules. Appropriate amounts of K^+ and Cl^- ions were added to reach the salt concentration of 150 mM at physiological levels. The NAMD[39] molecular dynamic package was used to perform all simulations in the NPT ensemble using 2 fs time steps, under periodic boundary conditions (PBC). Long-ranged electrostatic interactions were calculated with a Particle Mesh Ewald[51] (PME), and the cut-off distance of 12 Å was used for van der Waals and short-ranged electrostatic interactions. The SHAKE[52] algorithm was used to constrain bonds involving H atoms. In the NPT simulations, the temperature was controlled at 310 K using a Langevin dynamics thermostat, and the pressure was controlled at 1 bar using a Nose–Hoover–Langevin barostat with a damping time scale of 100 fs and a Langevin piston oscillation period of 200 fs.[53,54] VMD[40] was used for visualization and trajectory analysis.

3. Results

3.1. Equilibrated structure of isolated NPs

Fig. 2 shows the initial (left panel) and final equilibrated (right panel) configurations of the NPs in the absence of the membrane. For each system, the final equilibrated structure shows the 2 siRNAs stably bound together by 2 to 4 PEIs located in between ("bridging PEIs") while the rest of the PEIs are attached to the periphery of the NP ("peripheral PEIs"). The gyration radius (R_g) of the NP and the COM distance between the 2 siRNAs, which represent the compactness of the NP, are shown in Fig. 3. The horizontal time axis starts at 5 ns since the NP is subjected to restrained simulations with little structural changes during the first 5 ns. The R_g for all three systems shows a decreasing trend, ultimately reaching stable values of 24.07 ± 0.17, 25.44 ± 0.40 and 26.08 ± 0.31 Å (data collected from the last 20 ns) for native NP, LA-NP and CA-NP, respectively. The COM distance also shows a similar decreasing trend for LA-NP and CA-NP, indicating the siRNA molecules moving closer compared to their starting configurations. The 2 siRNAs in the native NP system, on the other hand, remain more

Table 1 Information on the simulated systems in this study

Number	System	Number of atoms	Size of simulation box (Å^3)	Lipid no./type on each PEI	Charge ratio PEI/siRNA	Simulation time (ns)
1	POPC	242 756	170 × 172 × 81	—	—	50
2	2siRNA-6PEIs (native NP)	106 042	109 × 100 × 104	None	1.5	50
3	2siRNA-6LA-PEIs (LA-NP)	112 598	93 × 118 × 109	3 LA	1.27	50
4	2siRNA-6CA-PEIs (CA-NP)	106 921	94 × 101 × 120	3 CA	1.27	50
5	(Native NP)-POPC	782 077	170 × 172 × 268	None	1.5	64
6	(LA-NP)-POPC	778 742	170 × 172 × 270	3 LA	1.27	64
7	(CA-NP)-POPC	778 859	170 × 172 × 270	3 CA	1.27	64

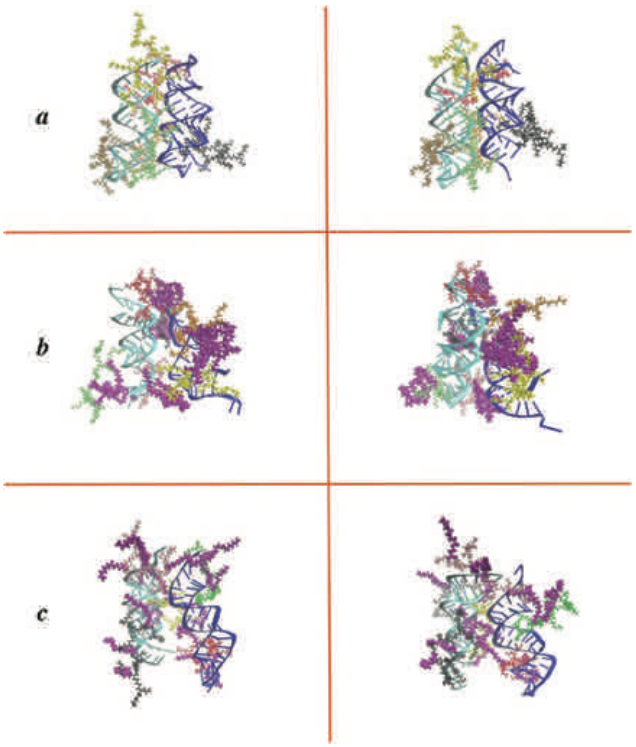

Fig. 2 Snapshots of initial (left panel) and final (right panel) configurations of the NPs in the absence of the membrane. (a) Native NP, (b) LA-NP, and (c) CA-NP. Different PEIs and siRNAs are represented by different colors; the lipid moieties on the PEIs are highlighted in purple; water and ions are removed for clarity.

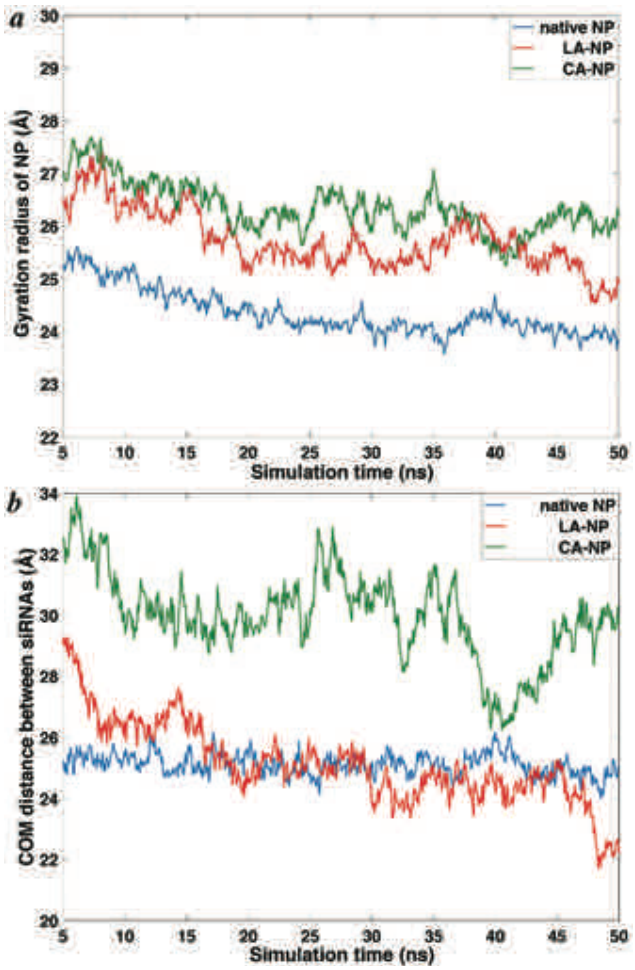

Fig. 3 (a) Radius of gyration of NPs and (b) the COM distance between the siRNA molecules as functions of the simulation time.

stable, with the COM distance deviating little from its starting value. The final COM distances, averaged over the last 20 ns, are 25.07 ± 0.38, 24.11 ± 0.79 and 29.14 ± 1.37 Å for native NP, LA-NP and CA-NP, respectively.

Based on Fig. 3, it can be concluded that CA-NP has the loosest equilibrium structure among the 3 systems. Compared with native NP, LA-NP has a larger R_g while its COM distance is slightly smaller. Via additional simulations, we confirmed that the observed phenomena are not caused by the chosen initial configurations (see details in the ESI, section S1†). Rather, these observations can be understood by examining the two competing factors brought about by the lipids grafted on the PEI: steric hindrance that prevents the formation of a compact structure and lipid association that favors compactness.[22,24,55] The final configuration of CA-NP in Fig. 2c shows that there is limited association between the CA lipids due to their short chain lengths. Therefore, compared with the native PEIs, the steric hindrance of the bridging PEIs caused larger separation of the siRNAs and consequently larger R_g. In the case of LA-NP, the association of the long-chained LAs is significant (see Fig. 2b), surpassing the influence of steric hindrance and leading to a COM distance even smaller than that of the native NP. The larger R_g of LA-NP as compared to native NP is due to the peripheral PEIs in which the long LA substitutions also show a high degree of association. The large amount of lipid association in LA-NP leads to a more rigid structure compared with native NP and CA-NP, which is expected to influence the configurational changes of the NP during membrane penetration.

3.2. Membrane penetration process

Fig. 4a shows the force profiles during the SMD simulations, plotted against the COM position of the NP. The two dashed lines mark the two surfaces of the original undeformed membrane. The membrane-crossing process in this figure can be divided into four stages: approach (−80 to −60 Å), attachment (−60 to 0 Å), embedment (0 to 50 Å), and detachment (50 to 80 Å). Fig. 5 shows side-view snapshots of the NPs and the membrane representative of each of these four stages. The corresponding COM positions of the NP are marked in Fig. 4a. Overall, the force profiles of the three systems show a similar trend. During the approach stage, the applied force is small and almost constant, which shows that the only resistance against the movement of the NP is due to the dissipative force caused by its friction with the solvent. In the attachment stage, the NP experiences additional resistance due to the presence

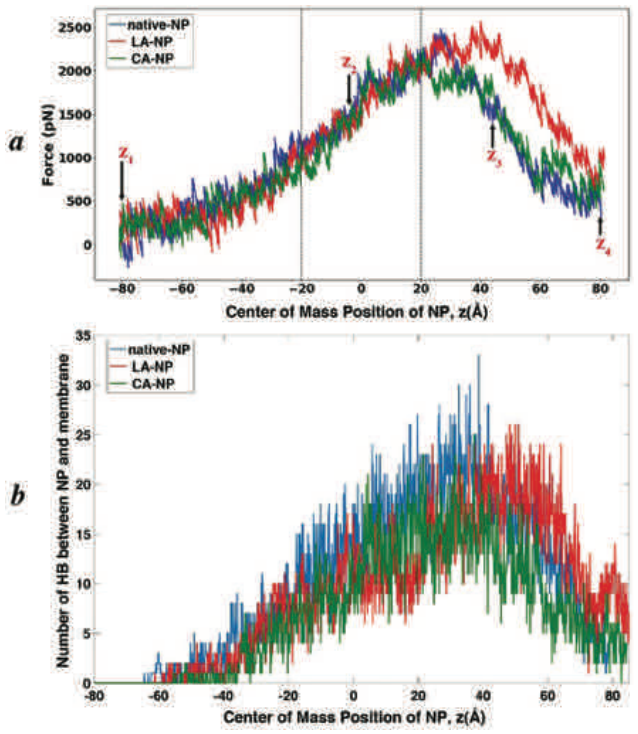

Fig. 4 (a) Force *vs.* COM position of the NP during SMD. The two dashed lines mark the surfaces of the initial undeformed membrane. Black arrows indicate the four locations where the snapshots in Fig. 5 are taken. (b) Number of HB between the NP and the membrane as a function of the COM position of the NP.

of the membrane and the applied force increases. Physically, this resistance originates from the necessity of deforming the membrane to allow for NP entry. The bi-layer structure of the membrane is maintained by the hydrogen bonds between the phosphate and amino groups on the two leaflets, as well as by the hydrophobic–hydrophobic interactions between the lipid tails located in the center. Attachment of the NP to the membrane causes bending of the membrane (Fig. 5) and disruption of those interactions. During the embedment stage, the rising trend of the applied force continues until a critical COM position is reached where the force is maximal. The magnitude of the peak force is only slightly different for the three NPs and the small difference is comparable to the fluctuations in the force profiles. This suggests that the maximum membrane resistance is insensitive to the lipid modification of the PEI carriers. After the peak value, the force decreases due to the visible formation of a pore in the membrane that facilitates further NP penetration (Fig. 5). The force continues to decrease in the detachment stage as the NP leaves the lower leaflet of the membrane. However, even at the end of the simulation (z = 80 Å), the force did not reduce to the levels seen in the attachment stage, indicating attractive interactions of the NP with the membrane (Fig. 5).

During the membrane-crossing process, as the NP establishes contact with the membrane, its exposure to water can be reduced. Such contact can be quantified by calculating the number of hydrogen bonds (HB) between the NP and the membrane, as shown in Fig. 4b. The HB between water and

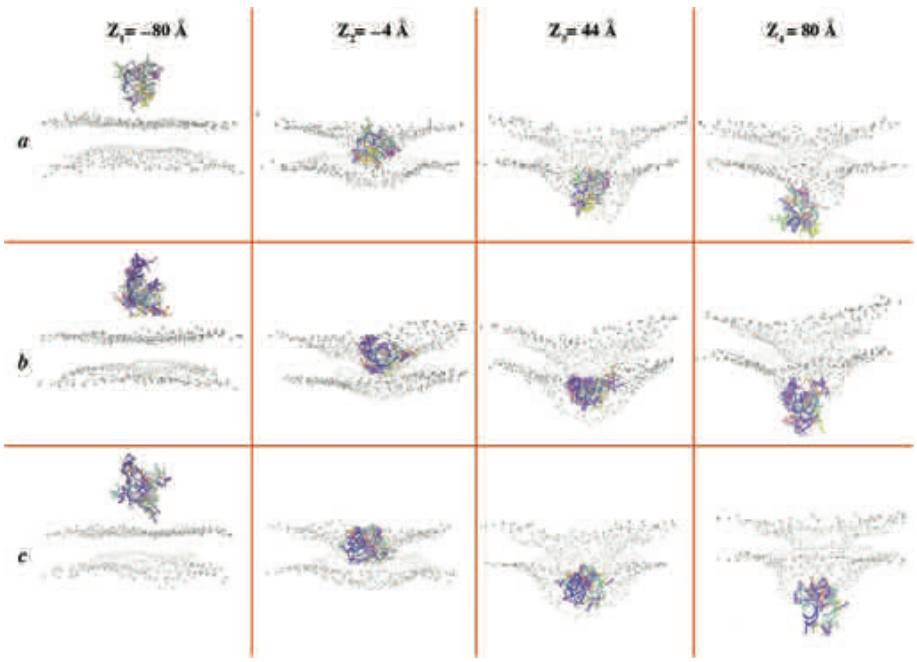

Fig. 5 Side-view snapshots of the NP and the membrane at different times of the SMD simulation: (a) native NP (b) LA-NP, and (c) CA-NP. Different PEIs and siRNAs are represented by different colors; lipid moieties on the PEIs are highlighted in purple; for clarity, water and ions are removed and only the phosphate (P) atoms of the membrane are shown (in gray). The four snapshots, from left to right, correspond to the simulation time of 0 ns, 30 ns, 50 ns and 64 ns, respectively. The corresponding positions of the NP COM are indicated on the top, and also marked in Fig. 4a.

the membrane, and between water and the NP are shown in Fig. S2 of the ESI.† A comparison between Fig. 4a and b shows a positive correlation between the force and the NP-membrane HB. During the approach stage, the number of HB is zero, indicating the lack of interaction between the NP and the membrane, consistent with the constant force in this stage. As the NP makes contact with the membrane during attachment and embedment, the number of HB between the NP and the membrane increases, along with the increase in the force. Ultimately during detachment, the number of HB shows a decreasing trend due to the separation of the NP from the membrane. At the end of the simulations, the HB counts are nonzero, indicating that the NPs are still in contact with the membrane.

Although the force and HB profiles in Fig. 4 are qualitatively similar among the three systems, the COM position at which the force reaches its maximum and begins to decrease is noticeably larger for the LA-NP system (around 40 Å as compared to 20 to 30 Å in the native NP and CA-NP systems). Consistently, the COM position at which the HB reach their maximum is also larger in the LA-NP system (around 50 Å as compared to 30 to 40 Å in the native NP and CA-NP systems). This indicates that pore formation and water translocation from one side of the leaflet to the other, induced by LA-NP, occur at a much deeper location within the membrane compared with native NP and CA-NP, and as a result its detachment stage is delayed. At the end of the simulation, both the force and HB counts are higher in the LA-NP system than in the other two systems, suggesting stronger contact between LA substituted PEIs and the membrane during detachment. The stronger contact is also evidenced by the extraction of some lipid molecules out of the membrane, which can be seen from the presence of lipid molecules at deep locations along the z-axis at the end of the penetration process (Fig. S3, ESI†).

It is of interest to point out that in Fig. 4b, the increase in the number of HB at the beginning of the embedment stage indicates that when the NP entered the interior of the membrane, it did not get surrounded by the hydrophobic tails of the bi-layer membrane. Otherwise, we would have seen the shielding of the interactions between the polar groups on the NP and the hydrophilic head groups of the membrane, which would have limited the HB formation. The membrane bent during the embedment and the lipid molecules re-oriented themselves to expose their head groups to the NP in order to facilitate the interaction. Kwolek *et al.*[30] studied the interaction of a PEI alone (in the absence of siRNA) with a membrane. They also observed that the phosphate groups of the membrane rearranged themselves to interact with the polar amine groups of the polymer, and this reorientation led to pore formation that allowed water to cross the membrane.

From the representative snapshots in Fig. 5, it is clear that although the NPs experienced some deformation during membrane penetration, they all maintained their overall integrity in this process. NP integrity during its membrane transport is critical to ensure full internalization of siRNAs. The configurational changes of the simulated NPs are assessed next by examining several parameters that describe the structural characteristics of the NPs during the penetration process.

3.3. Configurational changes of the NP during membrane penetration

To gauge the NP compactness, we plotted the R_g of the NP as a function of its COM position in each system (Fig. 6a). For all the three systems, the R_g curve starts from a relatively stable value in the approach stage (~24, 25 and 26 Å respectively for native NP, LA-NP and CA-NP), follows a decreasing trend in the attachment and embedment stages until reaching a minimum value, and ultimately finds an increasing trend in the detachment stage. This suggests that each NP undergoes some extent of compaction during attachment and embedment, and "recovers" from its compacted structure as it separates from the membrane. The most compact structures correspond to the R_g being around 22.5 Å for native NP and CA-NP, and around 23.5 Å for LA-NP. The relative compaction is smallest

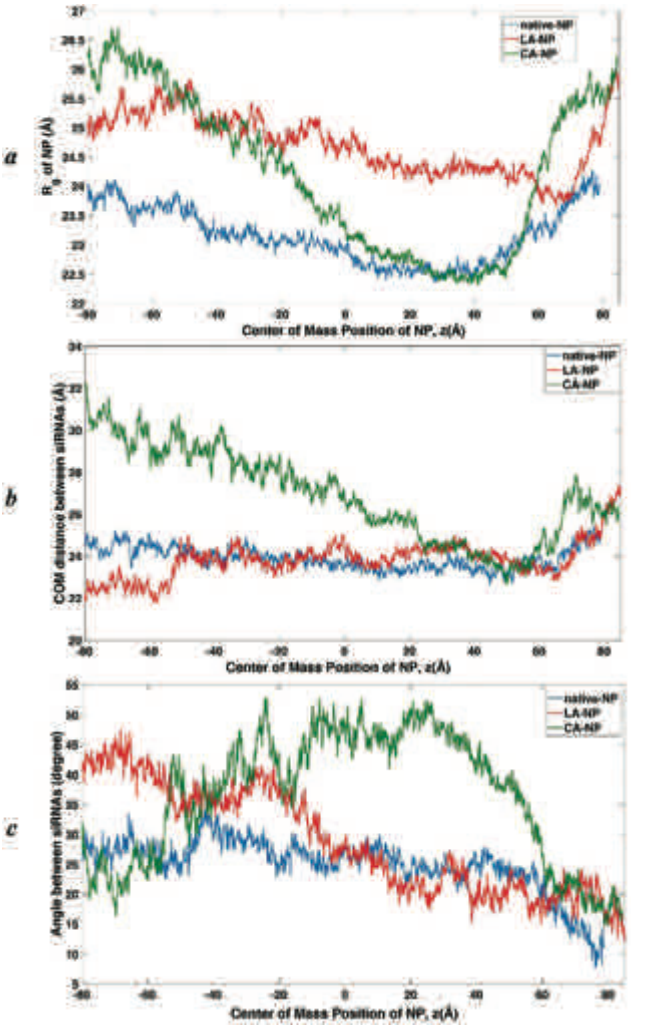

Fig. 6 (a) Gyration radius of the NP, (b) the COM distance between the two siRNA molecules, and (c) the relative angle between the two siRNA molecules, each as a function of the COM position of the NP.

for LA-NP (~6%), followed by ~7% for native NP and ~17% for CA-NP.

Additional evidence for NP compaction during penetration can be seen from Fig. 6b, which shows the COM distance between the 2 siRNAs as a function of the COM position of the NP. The trend of CA-NP is similar to its corresponding R_g curve in Fig. 6a, indicating significant compaction of the NP. For native NP, the COM distance is almost constant except for the detachment stage where it experiences a small increase. Together with the decrease in the R_g during attachment and embedment, the result suggests that the compaction of native NP occurs through the peripheral PEIs. For LA-NP, its COM separation exhibits some extent of increase during attachment; it then stays almost constant until the detachment stage. Interestingly, despite the very different initial COM separations, the three NPs attain similar COM separation when embedded in the membrane (~23.5 Å).

Visual examination of simulation trajectories also revealed rotation of the NPs while crossing the membrane. Misalignment of the principal axes of the two siRNA molecules may impact the NP stability by influencing (i) the bridging PEIs, and (ii) the area between two siRNAs accessible to destabilizing compounds such as heparin.[5] The relative orientation of the 2 siRNAs was monitored by measuring the angle (θ) between two vectors each defined in one siRNA (see section S4, ESI† for detail). $\theta = 0°$ corresponds to the siRNAs being parallel, whereas $\theta = 90°$ represents two siRNAs perpendicular to each other. Fig. 6c shows θ as a function of the COM position of the NP. For native NP, θ starts from ~28° and gradually decreases to ~15° at the end of the simulation. LA-NP shows a similar trend: while its initial θ is much larger (above 40°), the decrease in θ is also more significant, and the ultimate θ value is also ~15°. A different trend is observed for the CA-NP system: θ starts from ~25°, experiences an initial increase, reaches a maximum value of ~50° and ultimately decreases sharply to ~15°. Similar to the COM separation, while the NPs start from different angles between the 2 siRNAs, the final angles after crossing the membrane are similar, which corresponds to a relatively parallel orientation.

4. Discussion

4.1. Self-protecting configuration

Using SMD simulations, this study investigated the configurational changes of siRNA/PEI NPs during membrane penetration for the first time at an all-atom scale. We focused on a comparison of NPs derived from lipid-substituted PEIs, given the importance of these carriers in delivering siRNAs across cellular membranes.[56] We found that HB formation between PEI and the membrane molecules did not lead to the instability of NPs during the internalization process. In contrast, each NP was observed to undergo some degree of compaction during attachment and embedment stages. As the NP crosses the membrane, it introduces disruptions to the interactions among the lipid molecules of the membrane, causing the membrane to bend and inducing a pore in the membrane structure. The internalization of the NP therefore involves overcoming an energy barrier inherently dependent on the size of the NP. To minimize this energy barrier, the NP alters its stiffness and compacts during the embedment process. Yi *et al.*[57] previously noted that many viruses utilize their stiffness to facilitate the infection process, where they soften (expand) before uptake and harden (compact) before budding out of the host cells. The structure compaction is expected to protect the NP from being disintegrated by its interaction with the membrane molecules. In particular, it limits the interaction between the bridging PEIs and the membrane, stabilizing the siRNA/PEI NP while being present in the membrane. Another way to promote the stability of the NP, which has been observed from our simulations, is the re-orientation of the siRNA. In the case of two siRNAs simulated here, they were found to form a nearly parallel configuration at the end of the membrane–penetration process, which leads to a reduction in the area between the siRNAs accessible to destabilizing compounds, beneficial to enhancing the NP stability. Our results suggest the adoption of a "self-protecting strategy" by the NPs: during membrane penetration, they become more compact and the siRNAs are more parallel leading to a more stable configuration while detaching from the membrane.

Depending on the lipid substitutions on the PEI, different NPs showed different degrees of internal restructuring (compaction and re-orientation) during membrane crossing. The restructuring in native NP was mild: there was less than 10% reduction in the R_g, no reduction in the siRNA COM separation, and an insignificant change in the angle between the two siRNAs. LA-NP also showed little change in the siRNA COM separation, while there was a small degree of compaction of peripheral PEIs reducing the R_g. The low capacity of LA-NP for compaction is likely due to its high rigidity caused by significant association of the long-chained LA substitutions, especially among the bridging PEIs. Nevertheless, the LA-NP was able to enhance the NP stability by changing the relative orientation of the 2 siRNAs, which underwent a large change and became almost parallel. The CA-NP showed the largest changes in the compactness: it started with a much looser structure in the initial configuration due to non-associating CAs; both R_g and COM separation of the siRNAs decreased significantly to a level similar to those of native NP and LA-NP, which were originally much more compact. The angle between the two siRNAs increased during the compaction, but decreased to the same value as those of the other two NPs. The initial increase in the angle is likely due to the steric hindrance caused by the short CA substitution. In order to form a more compact structure, the COM separation of the siRNAs needs to decrease, which is resisted by the steric hindrance. To compensate for this, the angle between the 2 siRNAs increased to accommodate a more compact structure. Interestingly, while the 3 NPs start from very different values of initial COM distance and relative angle between the 2 siRNAs, they converge to similar values after crossing the membrane.

One important observation made in the past with CG simulations is the rotation of the NP as a whole, relative to the lipid bilayer, during its translocation.[58–62] Huang *et al.*[63] simulated the wrapping of spherocylindrical NPs with different aspect ratios by a lipidic membrane. For an aspect ratio of 2, the NP rotated from its initial upright docking position until it completely laid down with its long axis parallel to the membrane surface. The NP then stood up and was ultimately endocytosed with a nearly 90° entry angle. Here, although we simulated direct penetration instead of endocytosis, we also observed the rotation of the NP components in a similar manner (Fig. S5, ESI†). Fig. 7 shows the angle between each siRNA and the unperturbed membrane surface at the four NP locations where the snapshots in Fig. 5 are taken.

During attachment, the NP rotates to a more parallel configuration to allow for more HB formation between its peripheral PEIs and the membrane surface. This continues in the embedment stage accompanied by NP compaction and mutural re-orientation of the siRNAs. At the end, the NP rotates to a more perpendicular (standup) configuration to reduce the pore size in the detachment stage. The standup orientation is more evident in native NP and CA-NP than in LA-NP.

4.2. Implications

Our simulations revealed the configuration changes of siRNA/PEI NPs during penetration through a model membrane, which is inaccessible in experiments. Various experimental studies on the cellular uptake of LA and CA modified PEIs have shown improved efficiency of siRNA delivery with lipid substitutions as compared to native PEIs.[9,64,65] In an experimental study by Neamnark *et al.*,[66] the effect of different lipid substitutions on the transfection efficiency of PEI-mediated gene delivery was investigated. CA substitution was found to be less effective in transfection compared to other lipids including LA substitutions. While the mechanism of cellular uptake in those studies might be different from the direct penetration simulated in our study (*i.e.*, endocytosis), our results still provide insights into NPs that can undergo direct penetration, as well as the endosomal escape stage of polynucleotide NPs, in which the encapsulating lipid bilayer around the NP needs to be broken and the polynucleotides need to disassemble from the polymeric carrier to be transported to the appropriate sub-cellular compartment. Our simulation shows that LA-NP is very stable during the penetration process due to the strong intra-particle lipid association. Another origin of the stability of the LA-NP is the close-to-parallel orientation of its siRNAs that makes the

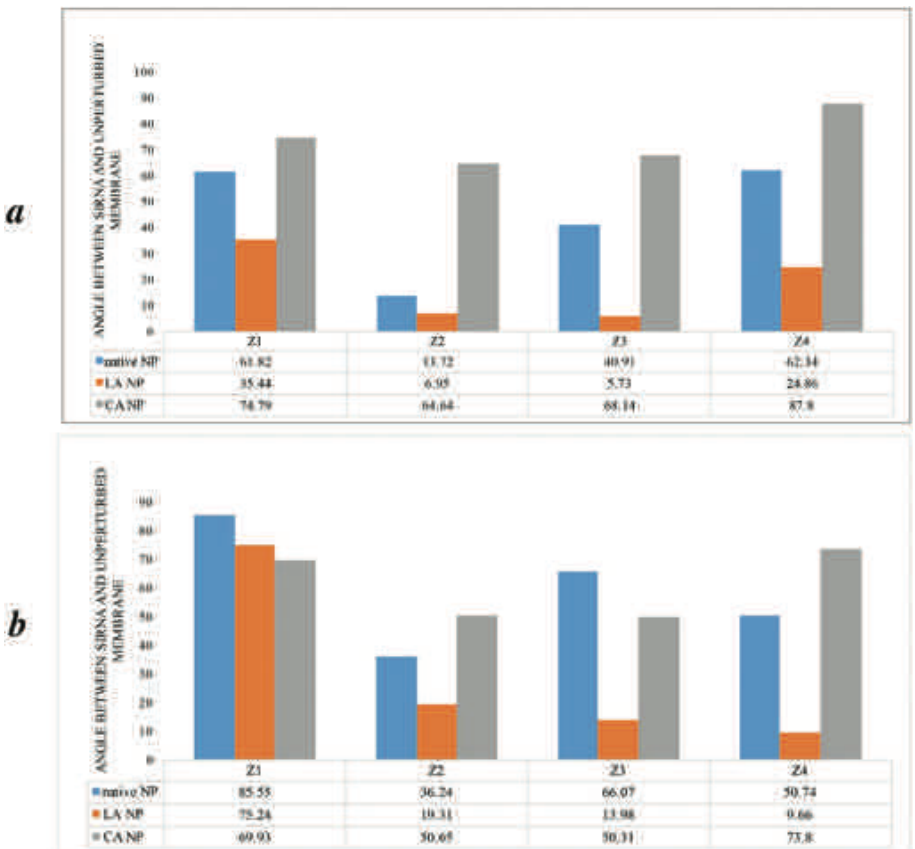

Fig. 7 Angle between (a) siRNA-1 and (b) siRNA-2 of NPs with an unperturbed membrane surface. Z_1, Z_2, Z_3, and Z_4 indicate the four locations where the snapshots in Fig. 5 are taken.

binding of destabilizing compounds such as heparin to the bridging PEIs difficult. Higher uptake and transfection ability of LA-NPs may be partially attributed to this enhanced stability. In the case of CA-NP, the observed increase in the relative angle between siRNAs may make the CA-NP more prone to dissociation during penetration. Usually the cell membrane surface contains destabilizing compounds such as heparin. Meneksedag-Erol *et al.*[5] proposed the following 5 stages for heparin mediated disassembly: (i) heparin binding to the NP, (ii) detachment of the surface PEIs, (iii) disengagement of the bridging PEIs, (iv) torsional change of siRNA and the subsequent relaxation of the NP, and (v) separation of siRNAs. The destabilizing compounds are more probable to attach to the bridging PEIs of CA-NP due to the creation of an accessible area between 2 siRNAs resulting from the increase in the relative angle between siRNAs, which could have contributed to the observed lower transfection efficiency of CA-NP compared to LA-NP in the experiments.

In the simulations performed here, the COM of the NP is restrained by SMD to mimic the process where the NP is pulled by certain external (*e.g.* electroporation) or biophysical forces towards the interior of the cell membrane. From Fig. 4a, it is seen that the required force for pulling the NP is positive throughout the process, indicating resistance from the membrane against NP penetration. Previous studies on polymer penetration through the membrane[14,20,67] have suggested that polymers with higher surface charge density and hydrophobic components are more likely to induce a pore in the membrane. The hydrophobic groups interact with the lipid tails and increase the fluctuations in the membrane, while the charged moieties make contact with the lipid head groups on the opposite leaflet. Such cooperative efforts lead to pore formation. For the three NPs investigated in this work, the native NP does not have any hydrophobic components, while the long LA lipids in LA-NP form strong association with themselves, which prevent them from interacting with the lipid tails in the membrane. In the case of CA-NP, the short CA lipids do not associate with themselves, but they are too short to establish sufficient contact with the lipid tails. Consequently, the membrane resisted the NP penetration and we did not observe attractive forces during attachment and embedment that could cause spontaneous pore formation. This analysis implies that the NP would not be able to move towards the interior of the membrane if the external restraint is removed. To confirm this, we performed a series of MD simulations in the absence of the pulling force (see details in the ESI, section S6†). In particular, a NP configuration obtained from the SMD simulation was first selected. Then, the restraint on the COM of the NP was removed and the system was simulated for 20 ns. Each NP was observed to move backwards (in the $-z$ direction in Fig. 4), away from the membrane. The tendency of the membrane to recover from its deformation and the more favorable interaction of the NP with water compared with the membrane eventually cause the previously induced pore to reseal.

To further strengthen the mechanistic understanding of NP performance, future MD simulations should be conducted for NPs with different charge ratios and different levels of substitutions, to examine whether proper assignments of those parameters might lead to forces driving the NP internalization. Simulations can also be done to assess the NP integrity and relative angle between siRNAs in the presence of destabilizing compounds, thus helping to better interpret the experimental results on silencing and transfection efficiency and eventually helping to screen more effective carriers.

4.3. Limitations

One of the general limitations with any all-atom MD simulation is the length and time scales that make it highly challenging to investigate the dynamics of real-size supramolecular assemblies. Current all-atom simulations allow simulations of systems involving $<10^6$ atoms for less than one μs, which is much smaller than those under real experimental conditions.[68] Considering the specific systems studied here, we recognize that the membrane penetration of the siRNA/PEI NP can take more than 64 ns as simulated in this work, and there might be configurational changes not entirely captured by our simulations. One approach to overcome the computational limit is to use CG approaches such as dissipative particle dynamics (DPD). In the DPD method, a cluster of atoms is treated as one soft spherical bead, whose motion is governed by the interactions among beads and certain collision rules, thus decreasing the degrees of freedom and enabling larger time steps. However, CG methods cause a loss of atomistic details of the simulated systems. While some of our observations were also made previously, for instance the reorientation of lipid head groups during pore formation as reported in both all-atom and CG simulations of cationic polymers,[30,69] the differences caused by lipid substitutions especially the significant structural change of CA-NP are intriguing and are of high interest for the design of siRNA carriers.

It is known that the pulling speed can impact the results of an SMD simulation. To test the sensitivity of our result to the pulling speed, we performed SMD simulations on the CA-NP using 5 and 10 Å ns^{-1} pulling speeds (see details in the ESI, section S7†). While the magnitude of force increases at a higher pulling speed, the qualitative trends remain the same. The self-protecting configuration, compaction and siRNA reorientation are all observed at all pulling speeds as well. Therefore, the choice of the pulling speed does not influence the trends drawn from this study.

In this work, we used a fixed N/P charge ratio for the NPs, and the maximum N/P ratio simulated was 1.5, while in practical applications, the N/P charge ratio ranged from 6 to 80 for siRNA/PEI NPs[64,70–72] to ensure full protection of the siRNA cargo during its delivery. Additionally, the size of our simulated NPs is ~3 nm, while the actual siRNA/PEI NPs are typically ~100 nm in diameter. However, it is not possible with the current computational power to simulate such large NPs with all-atom MD simulations.

Lipid bilayers are striking structures and their mechanical properties are crucial to the behavior of cell membranes.[73] However, they are not composed of a single type of lipid and

as many as 1000 different lipid species, with a variety of aliphatic chain lengths, head groups and other rigid structures, may exist in any eukaryotic cell membrane.[74] The glycerophospholipids including phosphatidylcholine (PtdCho), phosphatidylethanolamine (PtdEtn), phosphatidylserine (PtdSer), phosphatidylinositol (PtdIns) and phosphatidic acid (PA) are major structural lipids in eukaryotic membranes.[75] Among glycerophospholipids, PtdCho accounts for >50% of the phospholipids in most of the eukaryotic membranes.[75] The simulated zwitterionic POPC lipid bilayer here is from the PtdCho family, but one can always conduct simulations with other lipids and especially with a combination of them. Utilizing more complex membrane models will be beneficial for more realistic simulations, especially for investigating the effects of membrane constituents in terms of charge and hydrophobicity. This will be addressed in upcoming simulations.

5. Conclusions

The configurational changes of siRNA/PEI NPs during membrane penetration are studied from a series of SMD simulations for the first time at the all-atom scale. We developed an approach to study the effect of lipid substitutions (LA and CA) on the behavior of the NP. We found that, within the time scale of our SMD simulations, HB formation between PEI and the membrane molecules did not lead to NP instability during the penetration. Additionally, our results suggested the adoption of a "self-protecting" configuration by NPs during membrane penetration: the NPs become more compact and siRNAs more parallel leading to a more stable configuration while detaching from the membrane. Depending on the lipid substitutions, different NPs showed different degrees of internal restructuring (compaction and re-orientation). LA-NP showed the lowest change in compactness due to its high rigidity caused by the significant lipid associations among the long-chained LA substitutions. CA-NP showed the largest changes: it started with a much looser structure due to steric hindrance of non-associating CA substitutions, but underwent significant compaction accompanied by large changes in the relative orientation of the siRNAs to overcome the steric hindrance. These mechanistic observations provide unique insight into the internalization of siRNA/PEI NPs, and facilitate the design of new carriers for gene delivery.

Conflicts of interest

There are no conflicts to declare.

Acknowledgements

Compute Canada and Westgrid are gratefully acknowledged for providing the computing resources and technical support. This work is funded by Natural Sciences and Engineering Research Council of Canada (NSERC), Canadian Institutes of Health Research (CIHR) and Alberta Innovates-Technology Futures (AITF).

References

1 S. M. Elbashir, J. Harborth, W. Lendeckel, A. Yalcin, K. Weber and T. Tuschl, *Nature*, 2001, **411**, 494.
2 D. Castanotto and J. J. Rossi, *Nature*, 2009, **457**, 426.
3 M. Zheng, G. M. Pavan, M. Neeb, A. K. Schaper, A. Danani, G. Klebe, O. M. Merkel and T. Kissel, *ACS Nano*, 2012, **6**, 9447–9454.
4 A. S. Ansari, P. J. Santerre and H. Uludağ, *J. Mater. Chem. B*, 2017, **5**, 7238–7261.
5 D. Meneksedag-Erol, T. Tang and H. Uludağ, *Biomaterials*, 2018, **156**, 107–120.
6 D. Meneksedag-Erol, R. B. KC, T. Tang and H. Uludağ, *ACS Appl. Mater. Interfaces*, 2015, **7**, 24822–24832.
7 D. Fischer, Y. Li, B. Ahlemeyer, J. Krieglstein and T. Kissel, *Biomaterials*, 2003, **24**, 1121–1131.
8 V. Incani, A. Lavasanifar and H. Uludağ, *Soft Matter*, 2010, **6**, 2124.
9 H. M. Aliabadi, B. Landry, R. K. Bahadur, A. Neamnark, O. Suwantong and H. Uludağ, *Macromol. Biosci.*, 2011, **11**, 662–672.
10 H. Ding and Y. Ma, *Small*, 2015, **11**, 1055–1071.
11 S. Zhang, H. Gao and G. Bao, *ACS Nano*, 2015, **9**, 8655–8671.
12 J.-U. Sommer, M. Werner and V. A. Baulin, *EPL*, 2012, **98**, 18003.
13 M. Werner, J.-U. Sommer and V. A. Baulin, *Soft Matter*, 2012, **8**, 11714.
14 A. A. Gurtovenko, J. Anwar and I. Vattulainen, *Chem. Rev.*, 2010, **110**, 6077–6103.
15 D. P. Tieleman, *BMC Biochem.*, 2004, **5**, 10.
16 T. Kodama, A. G. Doukas and M. R. Hamblin, *Biochim. Biophys. Acta, Mol. Cell Res.*, 2002, **1542**, 186–194.
17 K. Koshiyama, T. Kodama, T. Yano and S. Fujikawa, *Biophys. J.*, 2006, **91**, 2198–2205.
18 A. A. Gurtovenko and J. Anwar, *J. Phys. Chem. B*, 2007, **111**, 10453–10460.
19 H. Leontiadou, A. E. Mark and S. J. Marrink, *J. Am. Chem. Soc.*, 2006, **128**, 12156–12161.
20 H. Lee and R. G. Larson, *J. Phys. Chem. B*, 2006, **110**, 18204–18211.
21 H. Nakamura and S. Watano, *KONA Powder Part. J.*, 2018, **35**, 49–65.
22 C. Sun, T. Tang and H. Uludag, *Biomaterials*, 2013, **34**, 2822–2833.
23 C. Sun, T. Tang and H. Uludağ, *J. Phys. Chem. B*, 2012, **116**, 2405–2413.
24 C. Sun, T. Tang and H. Uludağ, *Biomacromolecules*, 2012, **13**, 2982–2988.
25 Y. Li, X. Li, Z. Li and H. Gao, *Nanoscale*, 2012, **4**, 3768–3775.
26 Q. Xia, H. Ding and Y. Ma, *Nanoscale*, 2017, **9**, 8982–8989.

27 T. Yue, X. Wang, F. Huang and X. Zhang, *Nanoscale*, 2013, **5**, 9888.
28 X. Chen, D. P. Tieleman and Q. Liang, *Nanoscale*, 2018, **10**, 2481–2491.
29 K. Shimizu, H. Nakamura and S. Watano, *Nanoscale*, 2016, **8**, 11897–11906.
30 U. Kwolek, D. Jamróz, M. Janiczek, M. Nowakowska, P. Wydro and M. Kepczynski, *Langmuir*, 2016, **32**, 5004–5018.
31 A. Y. Antipina and A. A. Gurtovenko, *RSC Adv.*, 2016, **6**, 36425–36432.
32 C. K. Choudhury, A. Kumar and S. Roy, *Biomacromolecules*, 2013, **14**, 3759–3768.
33 M. Abbasi, H. M. Aliabadi, E. H. Moase, A. Lavasanifar, K. Kaur, R. Lai, C. Doillon and H. Uludağ, *Pharm. Res.*, 2011, **28**, 2516–2529.
34 M. Abbasi, A. Lavasanifar, L. G. Berthiaume, M. Weinfeld and H. Uludağ, *Cancer*, 2010, **116**, 5544–5554.
35 K. Utsuno and H. Uludağ, *Biophys. J.*, 2010, **99**, 201–207.
36 L. E. Gerweck, *Mol. Cancer Ther.*, 2006, **5**, 1275–1279.
37 Y. Kato, S. Ozawa, C. Miyamoto, Y. Maehata, A. Suzuki, T. Maeda and Y. Baba, *Cancer Cell Int.*, 2013, **13**, 89.
38 W. L. Jorgensen, *J. Am. Chem. Soc.*, 1981, **103**, 335–340.
39 J. C. Phillips, R. Braun, W. Wang, J. Gumbart, E. Tajkhorshid, E. Villa, C. Chipot, R. D. Skeel, L. Kalé and K. Schulten, *J. Comput. Chem.*, 2005, **26**, 1781–1802.
40 W. Humphrey, A. Dalke and K. Schulten, *J. Mol. Graphics*, 1996, **14**, 33–38.
41 R. D. Hills and N. McGlinchey, *J. Comput. Chem.*, 2016, **37**, 1112–1118.
42 N. Kučerka, S. Tristram-Nagle and J. F. Nagle, *J. Membr. Biol.*, 2006, **208**, 193–202.
43 J. M. Smaby, M. M. Momsen, H. L. Brockman and R. E. Brown, *Biophys. J.*, 1997, **73**, 1492–1505.
44 B. Israelewitz, J. Baudry, J. Gullingsrud, D. Kosztin and K. Schulten, *J. Mol. Graphics Modell.*, 2001, **19**, 13–25.
45 S. Z. Mousavi, S. Amjad-Iranagh, Y. Nademi and H. Modarress, *J. Membr. Biol.*, 2013, **246**, 697–704.
46 Q. Wei, W. Zhao, Y. Yang, B. Cui, Z. Xu and X. Yang, *ChemPhysChem*, 2018, **210009**, 1–14.
47 S. Park, F. Khalili-Araghi, E. Tajkhorshid and K. Schulten, *J. Chem. Phys.*, 2003, **119**, 3559–3566.
48 H. Nguyen, N. Do, T. Phan and T. Pham, *Appl. Biochem. Biotechnol.*, 2018, **184**, 401–413.
49 E. J. Denning, U. D. Priyakumar, L. Nilsson and A. D. Mackerell, *J. Comput. Chem.*, 2011, **32**, 1929–1943.
50 J. B. Klauda, R. M. Venable, J. A. Freites, J. W. O'Connor, D. J. Tobias, C. Mondragon-Ramirez, I. Vorobyov, A. D. MacKerell and R. W. Pastor, *J. Phys. Chem. B*, 2010, **114**, 7830–7843.
51 T. Darden, D. York and L. Pedersen, *J. Chem. Phys.*, 1993, **98**, 10089–10092.
52 J.-P. Ryckaert, G. Ciccotti and H. J. Berendsen, *J. Comput. Phys.*, 1977, **23**, 327–341.
53 G. J. Martyna, D. J. Tobias and M. L. Klein, *J. Chem. Phys.*, 1994, **101**, 4177–4189.
54 S. E. Feller, Y. Zhang, R. W. Pastor and B. R. Brooks, *J. Chem. Phys.*, 1995, **103**, 4613–4621.
55 S. Bagai, C. Sun and T. Tang, *J. Phys. Chem. B*, 2014, **118**, 7070–7076.
56 V. Incani, A. Lavasanifar and H. Uludağ, *Soft Matter*, 2010, **6**, 2124.
57 X. Yi, X. Shi and H. Gao, *Phys. Rev. Lett.*, 2011, **107**, 098101.
58 R. Vácha, F. J. Martinez-Veracoechea and D. Frenkel, *Nano Lett.*, 2011, **11**, 5391–5395.
59 Y. Liu, B. Peng, S. Sohrabi and Y. Liu, *Langmuir*, 2016, **32**, 10136–10143.
60 K. Yang and Y.-Q. Ma, *Nat. Nanotechnol.*, 2010, **5**, 579–583.
61 K. Yang and Y. Ma, *Aust. J. Chem.*, 2011, **64**, 894.
62 Y. Li, T. Yue, K. Yang and X. Zhang, *Biomaterials*, 2012, **33**, 4965–4973.
63 C. Huang, Y. Zhang, H. Yuan, H. Gao and S. Zhang, *Nano Lett.*, 2013, **13**, 4546–4550.
64 H. M. Aliabadi, B. Landry, P. Mahdipoor, C. Y. M. Hsu and H. Uludağ, *Eur. J. Pharm. Biopharm.*, 2012, **81**, 33–42.
65 H. Montazeri Aliabadi, B. Landry, P. Mahdipoor and H. Uludağ, *Mol. Pharm.*, 2011, **8**, 1821–1830.
66 A. Neamnark, O. Suwantong, R. B. KC, C. Y. M. Hsu, P. Supaphol and H. Uludağ, *Mol. Pharm.*, 2009, **6**, 1798–1815.
67 S. Pogodin, M. Werner, J.-U. Sommer and V. A. Baulin, *ACS Nano*, 2012, **6**, 10555–10561.
68 D. Meneksedag-Erol, T. Tang and H. Uludağ, *Biomaterials*, 2014, **35**, 7068–7076.
69 H. Lee and R. G. Larson, *J. Phys. Chem. B*, 2008, **112**, 12279–12285.
70 L. Wightman, R. Kircheis, V. Rössler, S. Carotta, R. Ruzicka, M. Kursa and E. Wagner, *J. Gene Med.*, 2001, **3**, 362–372.
71 M.-E. Bonnet, P. Erbacher and A.-L. Bolcato-Bellemin, *Pharm. Res.*, 2008, **25**, 2972–2982.
72 J. Valencia-Serna, H. Gul-Uludağ, P. Mahdipoor, X. Jiang and H. Uludağ, *J. Controlled Release*, 2013, **172**, 495–503.
73 D. P. Tieleman, H. Leontiadou, A. E. Mark and S.-J. Marrink, *J. Am. Chem. Soc.*, 2003, **125**, 6382–6383.
74 M. Sud, E. Fahy, D. Cotter, A. Brown, E. A. Dennis, C. K. Glass, A. H. Merrill, R. C. Murphy, C. R. H. Raetz, D. W. Russell and S. Subramaniam, *Nucleic Acids Res.*, 2007, **35**, D527–D532.
75 G. van Meer, D. R. Voelker and G. W. Feigenson, *Nat. Rev. Mol. Cell Biol.*, 2008, **9**, 112–124.

